# State-selective *K-K* electron transfer and *K* ionization cross sections for Ar and Kr in collisions with highly charged C, O, F, S, and Cl ions at intermediate velocities

B. B. Dhal,[1,*] Lokesh C. Tribedi,[1,†] U. Tiwari,[1] K. V. Thulasiram,[1] P. N. Tandon,[1] T. G. Lee,[2]
C. D. Lin,[2] and L. Gulyás[3]

[1]*Tata Institute of Fundamental Research, Homi Bhabha Road, Colaba, Mumbai 400 005, India*
[2]*JR Macdonald Laboratory, Department of Physics, Kansas State University, Manhattan, Kansas 66506*
[3]*Institute of Nuclear Research of the Hungarian Academy of Science (ATOMKI), P.O. Box 51, H-4001 Debreccen, Hungary*

We have measured the single *K-K* electron-transfer cross sections along with the single *K*-shell ionization cross sections of Ar induced by H-like and bare C,O, and F projectiles, and of Kr by F, S, and Cl ions in the energy range 1.5–6 MeV u$^{-1}$. The target x-ray yields as a function of the number of *K* shell vacancies in the incident beam were used to derive the *K* ionization cross sections of the targets and the *K-K* (i.e., target *K* shell to projectile *K* shell) electron-transfer cross sections. The enhancement in the fluorescence yield due to multiple vacancies in the target atom was deduced from the energy shifts and intensity ratios of the characteristic x-ray lines to derive vacancy production cross sections from the measured x-ray production cross sections. The energy shifts of *K* x-ray lines were found to be dependent on the incident charge states of the projectiles. Continuum-distorted-wave eikonal-initial-state calculations are found to underestimate the ionization cross-section data in general, and the deviations are most pronounced for Kr. Perturbed stationary-state calculations, including corrective terms due to energy loss, Coulomb deflection, and relativistic wave function, agree with the data only for asymmetric collisions ($Z_1/Z_2 \lesssim 0.4$), and largely overestimate for relatively symmetric systems. The *K-K* electron-transfer cross sections are well reproduced by the two-center close-coupling calculations for both targets except, for the asymmetric collisions. The perturbed stationary state (PSS) calculations of Lapicki and McDaniel are also used to explain the *K-K* electron-transfer data for the asymmetric systems. In addition, the *K-L* electron-transfer cross sections are also measured for S and Cl ions on Kr, and compared with the PSS calculations.

PACS number(s): 34.50.Fa, 34.70.+e

## I. INTRODUCTION

Ionization, electron capture, and excitation are among the most important inelastic processes in ion-atom collisions. At intermediate velocities, i.e., when the projectile velocity ($v_p$) is approximately equal to the orbital velocity ($v_e$) of the active electron, the strengths of these processes are of the same orders of magnitude, and a coupling among these different channels become important. Ionization and electron transfer involving deeply bound inner shells play major roles in producing vacancies in these shells in heavy ion-atom collisions. In some cases, depending on the symmetry parameter of the collision system the electron-transfer channel could be much larger than the direct Coulomb ionization. There have been numerous studies on the total electron capture of the initially loosely bound electrons, and several empirical scaling laws [1,2] have been proposed to predict the capture cross sections which are found to fall rapidly ($\sim v_p^{-11}$) with the projectile velocity. On the other hand, for the projectiles with energies of the order of magnitude of hundreds of MeVs, the cross sections for a deeply bound electron transfer (such as $\sigma_{K-K}$) process are expected to reach a maximum, since the projectile velocity ($v_p$) is approximately the same as the orbital velocity ($v_e$) of the ac-

tive electron, as in the present studies. State-selective electron-transfer cross sections involving deeply bound initial and final states cannot be described by such empirical laws, and the mechanism of such transfer processes in strongly perturbative collisions is not yet completely understood. The initial- and final-state binding energies of the transferred electron, the symmetry parameter $S_z = Z_1/Z_2$, and the reduced velocity $v_r = v_p/v_e$ of the collision system are the relevant parameters which are generally used to describe the transfer process. Here $Z_1$ and $Z_2$ refer to the atomic numbers of the projectile and the target, respectively. The binding energy matching between the initial and final states provides a favorable condition for the electron-transfer process, as predicted by first-order calculations.

Single *K-K* electron-transfer cross sections have been measured in a few cases in the past, and mostly using solid targets [3–6], in which the evolution of the vacancy configurations due to multiple collisions inside the target complicated the data analysis. A three-component model is generally used (see references in Ref. [7]) to fit the observed thickness dependence of the x-ray yields for different initial-charge states of the projectiles. These curves are then projected at zero thickness in order to extract the ionization and the electron-transfer cross sections. Some measurements are even carried out with a single thin target, and, as the measured values of the electron-transfer cross sections are quite large, the reported values might be dependent on the thickness of the target used due to the initial very steep thickness dependence of the charge states of the ion inside the solid. This is certainly true for incident charge states of the incident

*Present address: School of Physics, University of Melbourne, Parkville, Vic-3052, Australia.

†Corresponding author: Email address: lokesh@tifr.res.in

ions beyond their equilibrium values in solids [3,5,7]. There-fore, it is desirable to have measurements of these processes in which the single-collision condition is satisfied. This re-quires the use of gas targets at a low pressure. However, such experimental data are very sparsely available. We have, therefore, carried out measurements on single *K-K* electron-transfer cross sections in the intermediate velocity range $(0.2 \leqslant v_r \leqslant 1.2)$, where these cross sections are expected to be near the maximum. The measurements were pursued for dif-ferent values of symmetry parameters varying between 0.25 and 0.5. In addition, we have also included recent data [8] on *K-K* electron-transfer cross sections for the nearly symmetric collision $(S_z = 0.78)$ system of a Si projectile on an Ar target, for which a large enhancement in the double *K-K* electron-transfer channel has been observed.

In the case of ionization of strongly bound *K*-shell elec-trons by heavy projectiles, the first Born calculations are known to be unsuccessful in predicting the total cross sec-tions. In order to improve the situation, in one approach, Brandt and co-workers [9,10] developed the ECPSSR model based on the perturbed-stationary-state (PSS) approximation. In fact, in the case of *K*- and *L*-subshell ionization, it has become conventional to use the ECPSSR model, which is a first-order Born calculation, modified to include the correc-tions due to enhanced binding energy, the Coulomb (*C*) de-flection, the energy loss (*E*), and any relativistic (*R*) effects [9]. We will compare the calculations based on this model with our experimental data obtained for different symmetry parameters.

The electrons emitted in the heavy-ion-induced ionization are subject to long-range Coulomb interactions with recoil ions and projectiles. Theoretical models based on the continuum-distorted-wave (CDW) approximation have been developed [11,12] in order to explain such a two-center ef-fect on ionization. In the CDW approximation the initial and final unperturbed target wave functions are distorted by a projectile continuum factor. In one of its simplified versions known as CDW-EIS (EIS stands for eikonal initial state), originally developed by Crothers and McCann [13], the final state is chosen as in the CDW but the initial distorted state is represented as a bound state multiplied by a projectile eiko-nal phase (eikonal initial state) [14,15]. It was recently shown that the CDW-EIS model has been quite successful in explaining the angular distributions of electron double-differential cross sections in fast ion-atom ionization [16–19]. However, in the present collision systems the electrons are much more strongly bound $(v_r \leqslant 1)$, and it is not clear whether the CDW-EIS calculations can explain the ioniza-tion data for such highly nonperturbative collision systems. Therefore, we have also compared the experimental data on *K*-shell ionization with CDW-EIS calculations which employ the Hartree-Fock-Slater wave functions for initial and final states of the ionized electron.

It is well known that first-order calculations based on the OBKN (Oppenheimer-Brinkman-Kramer-Nikoleav) approxi-mation [20] overestimate the cross sections by a large factor. In the perturbed stationary-state approach, Lapicki and McDaniel [21] included a second Born term, and corrections due to the enhanced binding energy and the Coulomb deflec-

tion in the OBKN formalism, in the same way as was done in the ECPSSR formalism for ionization. This formalism is not an *ab initio* one, but the simplicity of using an analytical expression in this method, and its ability to predict cross sections for asymmetric collisions, makes it worth mention-ing. We would compare the calculations using this model with the experimental data as a function of the symmetry parameter, varying between 0.33 and 0.8.

A two-center semiclassical close-coupling method [22,23], based on atomic-orbital expansion [24], is found to be quite successful in explaining the state-selective electron-transfer cross sections, at least for the loosely bound outer-shell electrons. In this model the motion of the projectile is approximated by a classical trajectory, and the target elec-trons are treated quantum mechanically. For treating electron capture from the inner shells, an independent-electron model is used, and the active electron is described by a model po-tential fitted so that the binding energies of the inner-shell electrons are reproduced. Although the possible role of the outer-shell electrons (the so-called Pauli exchange effect) is not included explicitly in the theory, it may be partially ac-counted for in using the model potential. In the close-coupling calculation all the atomic states up to $n = 2$ on both centers have been included.

Here we present a series of measurements on the total *K*-shell ionization cross sections and the *K-K* electron-transfer cross sections for highly charged C, O, F, and Si ions on Ar, and F, S, and Cl ions on Kr. The energy of the various beams varied between 1.5 and 6 MeV/u. In the present experimental technique (as described below), we measure the charge state dependence of the target *K* x-ray production cross sections, and this allows us to extract the cross sections of the two major channels i.e., the *K-K* elec-tron transfer and the *K* ionization, in the same experiment.

## II. EXPERIMENTAL DETAILS

Ion beams of $^{12}$C, $^{16}$O, $^{19}$F, $^{32}$S, and $^{35}$Cl, at energies varying between 1.5 and 6 MeV/u, were obtained from the BARC-TIFR Pelletron accelerator at TIFR, Mumbai. The mass- and energy-analyzed beam was passed through a post-acceleration foil stripper to obtain different charge states of the incoming beam at a given energy. The highly collimated beam interacted with the desired gas targtet (Ar or Kr) in a cylindrical gas cell of length 4 cm. The entrance and exit apertures of diameters 3 and 3.5 mm, respectively, of the gas cell were electrically isolated. The beam current on these apertures was monitored in order to facilitate good beam transmission. The emerging beam was collected on a long extended Faraday cup connected to the chamber. The charge collected on the Faraday cup was used for normalization. The cell was differentially pumped, and the gas inflow con-tinuously monitored and controlled at a desired gas pressure in the cell with the help of a capacitance manometer and a solenoid valve. The base pressure in the main chamber was maintained at $1 \times 10^{-6}$ torr. The emitted x rays were de-tected at 90° with respect to the incident beam by two Si (Li) detectors through mylar windows of thickness 15 $\mu$m on the gas cell and 25 $\mu$m on the main chamber. Both the detectors
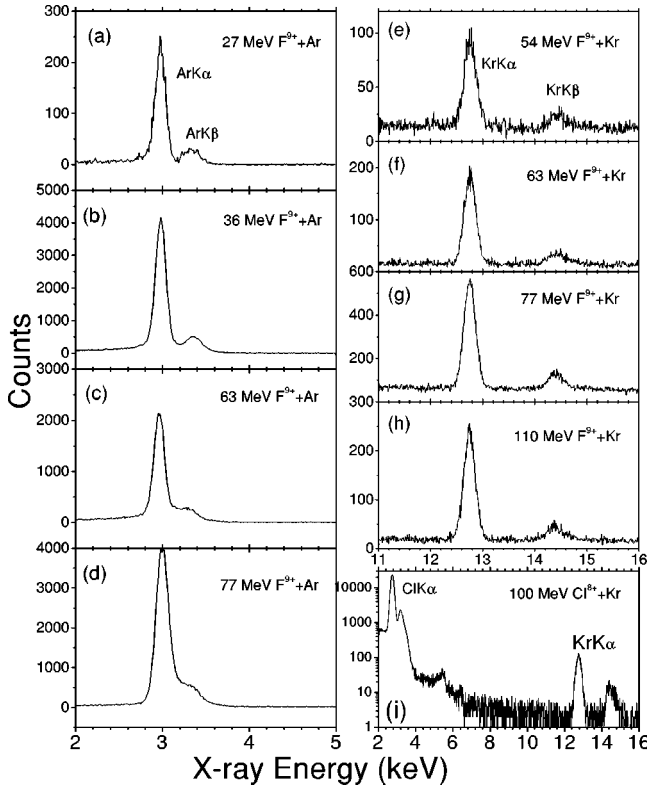
FIG. 1. The measured x-ray spectra on bombardment with F and Cl ions with different energies on Ar and Kr targets.



FIG. 2. The energy shifts ($\Delta E_\alpha$ and $\Delta E_\beta$) of Ar and Kr $K$ x rays as a function of the initial charge state of the projectile at various energies. The dotted lines are to guide the eyes, and the solid lines in (b) show the $q^2$ dependence. In (f), (g), and (h), $\langle \Delta E_\alpha \rangle$ or $\langle \Delta E_\beta \rangle$ represent the average shifts over various beam energies, since the shifts were observed to be almost independent of the beam energies (within about 10–20 eV) for the Kr target.

had a resolution of $\sim 160$ eV at 5.9 keV. A PC-based system along with a CAMAC controller was used for the data acquisition. An aperture was used in front of the detector to define the interaction volume in the gas cell accurately. The thickness of the mylar foil used was determined by measuring the transmission of 3.3-keV x rays from an $^{241}$Am source. The x-ray yield from the interaction volume was measured as a function of the gas pressure in order to ensure the single-collision condition. Typical values of the gas pressure used were about 5 mTorr for Ar and about 3 mTorr for Kr gas.

## III. DATA ANALYSIS, RESULTS, AND DISCUSSION

Typical x-ray spectra obtained for Ar on impact with F ions with different energies are shown in Figs. 1(a)–1(d). At the lowest beam energy used, i.e., for 27 MeV, the $K\alpha$ and $K\beta$ lines are quite well separated, but at higher energies the separation between the two lines is reduced. This reduction is associated with the multiple vacancies produced in the outer shells of the target atom, and is discussed below. The $K\alpha$ and $K\beta$ lines for the Kr target, however, are very well resolved, and some examples are shown in Figs. 1(e)–1(h). A typical x-ray spectrum for Cl+Kr is also shown in Fig. 1(i). The normalized intensity of the x-ray yield, corrected for the absorption in the mylar windows, and the Be window of the detector were used for obtaining the total $K$ x-ray production cross sections. The cross-section values obtained using the two detectors agreed with each other to within 5 to 10%. For absolute normalization, the Ar K x-ray yield was
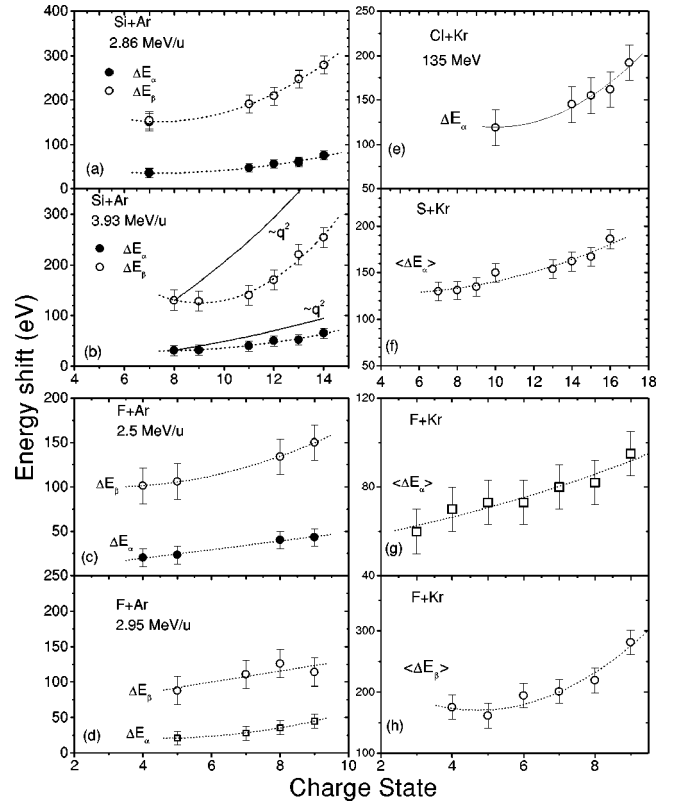
measured, in the same geometry, using 56- and 77-MeV F-ion beams in different charge states for which the x-ray production cross sections are known [25]. It was found that the cross sections derived from the present measurements were slightly lower than those obtained by Hopkins *et al.* However, we have used the existing data of Hopkins *et al.* [25] to normalize our cross-section data.

The energies of the $K\alpha$ and $K\beta$ components of the Ar and Kr $K$ x rays were found to be higher than the line diagram values [26], due to the presence of multiple vacancies in the higher shells simultaneous with the $K$-shell vacancy. The shifts in the energies of the $K\alpha$ ($\Delta E_\alpha$) and $K\beta$ ($\Delta E_\beta$) lines, together with their intensity ratios, were used to calculate the number of vacancies [27] in the $L$ and $M$ shells at the time of x-ray emission. This was required for estimating the fluorescence yield ($\omega_K$) of the target atoms. Figures 2(a)–2(h) show the charge-state dependence of the $\Delta E_\alpha$ and $\Delta E_\beta$ for Ar or Kr targets with different projectiles. The uncertainties in the peak energies of the $K\alpha$ and $K\beta$ lines were estimated to be $\sim 10$ and $\sim 20$ eV for Ar, and higher for Kr. It can be seen from Fig. 2 that for a given energy of the beam a definite increase in the energy shifts of the $K\alpha$ and $K\beta$ x-rays with the incident charge states ($q$) of the projectile is obvious. This observation reflects the $q$-dependent multiple vacancy production in the $L$ and $M$ shells. Apart from multiple

ionization there could also be single and multiple transfers of the *L*- and *M*-shell electrons from the target atoms to the vacant shells of the projectiles. The multiple-electron-transfer cross sections are much smaller than the single-electron-transfer cross sections, which are known to increase as $\sim q^{3.9}$ [1]. However, in the present case the binding-energy matching consideration is not favorable for a large *L-K* or *M-K* transfer. It may be mentioned here that in the case of solid targets such a dependence on charge states is not observed, since the outer shells of the projectiles reach equilibrium very quickly in a few layers of the solid. The observed charge-state dependence [Fig. 2(b)] is much slower than the predicted $q^2$ behavior by the Bethe formula for single ionization in the dipole approximation [28]. It is found that the data can be fitted with a polynomial in $q$, with non-dipole terms signifying the existence of a contribution from higher-order (nondipole) processes in the Born series for multiple ionization. This is qualitatively consistent with the observed q dependence of double (and multiple) ionization cross sections for heavy ions on He [29–31].

For a given charge state of the incident projectile, the shifts in both $K\alpha$ and $K_\beta$ for the Ar target show a decreasing trend with increasing projectile energy [see Figs. 3(a) and 3(b)]. The energy shifts $\Delta E_\beta$ fall faster than $\Delta E_\alpha$. It may be mentioned here that in the present collision systems the beam energy is higher than the energies at which one will expect the target *M*- and *L*-shell ionization cross sections to have maxima, and therefore both the *M*- and *L*-shell ionization cross sections are expected to fall as the incident beam energy increases. For example, the reduced velocity $v_r = v_p/v_e$ is about 1.2–2.5 for the *L* shell and 4–7 for the *M* shell for Ar in the present velocity range, and one expects that peak in the ionization cross sections would arise at around $v_r \approx 1.0$. This also explains the steeper fall of the $\Delta E_\beta$, which originates due to multiple vacancies present in the *M* shell, as the number of such vacancies decreases as the beam energy increases in the present energy range. In the case of a Kr target, the *L* and *M* shells are more strongly bound than for Ar, and the shifts show almost no energy dependence.

For the Ar target the energies of the $K\alpha$ and $K\beta$ lines increase by $\sim 20$ and $\sim 50$ eV, respectively, per vacancy in the *L* shell [27]. For a given *L*-shell vacancy, the increase due to the increasing number of vacancies in the *M* shell is calculated to be $\sim 3$ and $\sim 10$ eV per vacancy for the $K\alpha$ and $K\beta$ transitions, respectively. From the measured shifts and intensity ratios of the $K\alpha$ and $K\beta$ lines the number of vacancies were estimated to vary between 2 and 4 for the *L* shell and upto 5 for the *M* shell. The calculated values of the fluorescence yields $[\omega_K(q)]$ were found to be about 10–15% larger [27] than the single hole values (0.12) in the case of C, O, and F ions impinging on Ar. However, in the case of Si+Ar collision system, the enhancement in the fluorescence yield was about 10−25%. In the case of Kr target the fractional shifts in the x-ray energy (i.e., $\Delta E_\alpha/E_\alpha$) is much smaller than those for the Ar target for a given beam, implying that the enhancement in the value of $\omega_K$ would be quite small in the case of Kr. Therefore, we have used the single-hole fluorescence yield for Kr which may give rise to an
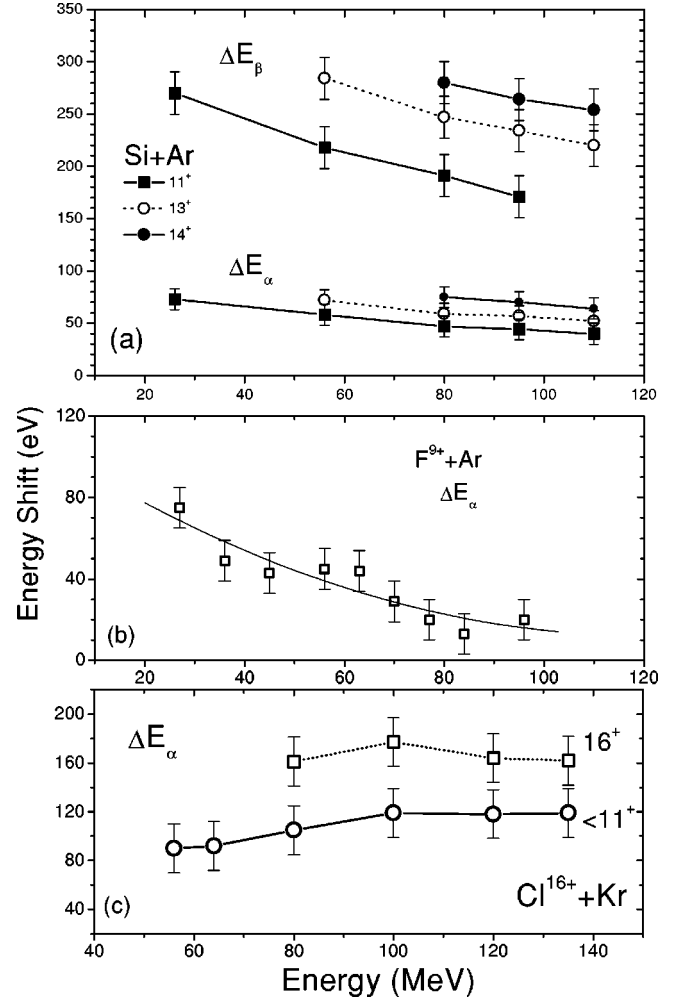


FIG. 3. (a) The energy shifts $\Delta E_\alpha$ and $\Delta E_\beta$ of the normal component of the Ar *K* x rays as a function of the energy of the projectile for three different charge states, i.e., $11^+$ (squares), $13^+$ (open circles) and $14^+$ (filled circles). The lines are to guide the eyes. The energy dependences of $\Delta E_\alpha$ (b) for F+Ar and (c) for Cl+Ar.

additional error of about 5% in the derived cross-section values.

The *K-K* electron-transfer cross sections were derived from the measurements of the *K* vacancy cross sections as a function of different charge states, i.e., with and without a *K* vacancy in the projectile. The *K* vacancy cross sections ($\sigma_{KV}$) were derived from the *K* x-ray cross section ($\sigma_{KX}$) using the deduced values of $\omega_K(q)$, i.e., from $\sigma_{KV}^i = \sigma_{KX}^i/\omega_K(q)$. The superscript $i$ ($i=0$, 1, and 2) refers to the number of *K*-shell vacancies in the incident ion. The charge-state dependences of $\sigma_{KV}$, measured at some energies, are shown in Figs. 4 and 5 for Ar and Kr targets, respectively. It is found that, in general, the $\sigma_{KV}$ data are almost independent of the charge states of the projectiles with filled K shell. However, in the case of heavier projectiles (e.g., Cl+Kr) one observes a slight increase in $\sigma_{KV}$ as a function of the number of *L* vacancies in the projectile. This increase is associated with the (target) *K* to (projectile) *L* (*K-L*) electron-transfer process, and from this variation we have also derived the
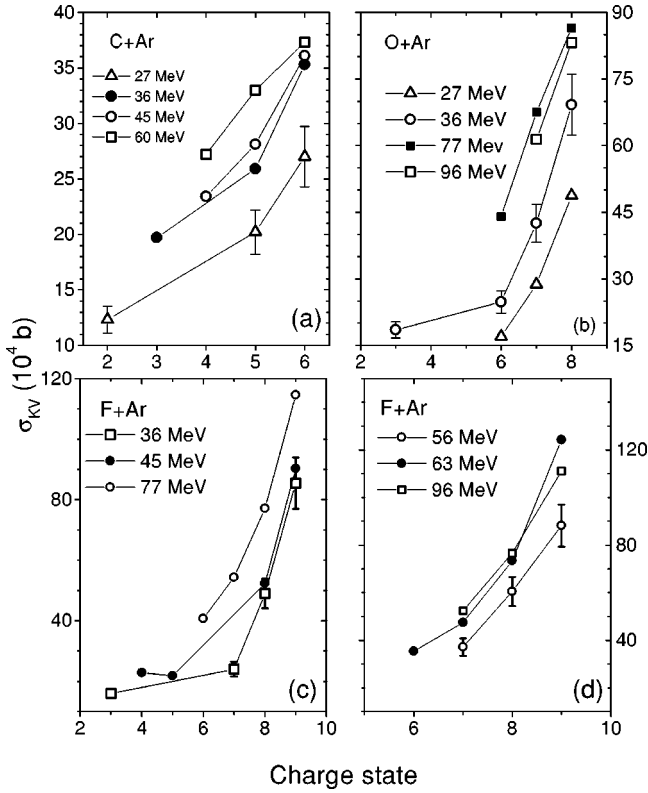
FIG. 4. The *K* vacancy production cross sections $\sigma_{KV}$ for Ar, as a function of the initial charge state of different projectiles. The data are shown for different energies, as indicated in the figures. The line joining the points is to guide the eyes only.

*K-L* transfer cross section per *L* vacancy ($\sigma_{K-L}$). A distinct increase in the cross sections for the He-like beams is associated with the metastable state of the He-like projectile ions, while the sudden rise in the vacancy production cross sections for the H-like and the bare ions is due to the direct *K-K* (i.e., from the *K* shell of the target to the *K* shell of the projectile) electron-transfer channel. The *K* ionization cross sections ($\sigma_{KI}$) are given by the *K* vacancy cross sections derived for beams with zero *K* vacancy ($\sigma^0_{KV}$) in the initial state i.e., $\sigma_{KI} \equiv \sigma^0_{KV}$.

The single and the double *K-K* electron-transfer cross sections were then deduced using the relations

$$\sigma_{K-K} = \sigma^1_{KV} - \sigma^0_{KV}, \tag{1}$$

$$\sigma_{K-K} = \frac{1}{2}(\sigma^2_{KV} - \sigma^0_{KV}). \tag{2}$$

It may be noted that the *K-K* electron-transfer cross section can be derived either from Eq. (1) or (2), and that the derived cross sections from these two equations are generally the same if the double *K-K* electron-transfer cross section is quite small compared to the *K-K* electron-transfer cross section [8], as in the present case.

The *K* ionization cross sections ($\sigma_{KI}$) are compared with the ECPSSR calculations (see Figs. 6 and 7). In Figs. 6(a)–6(d) we display these cross sections for C, O, F, and Si ions
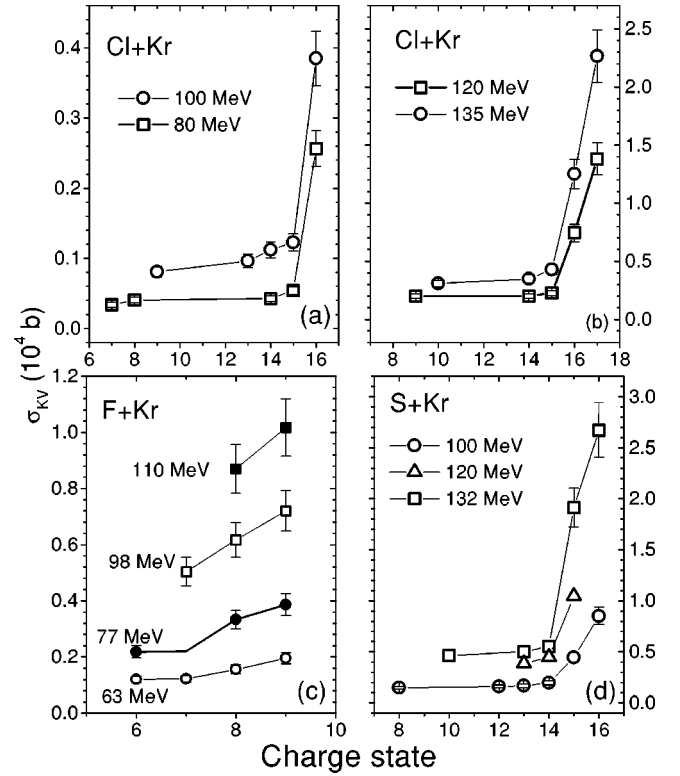


FIG. 5. The *K* vacancy production cross sections $\sigma_{KV}$ for Kr, as a function of the initial charge state of F, S, and Cl projectiles. The data are shown for different energies. The line joining the points is only to guide the eyes.

on Ar targets, i.e., for the symmetry parameter $S_z$ varying between 0.33 and 0.78. The data for Si+Ar (taken from Ref. [8]) have been included for a coherent discussion over a wide range of $S_z$ value. For the most asymmetric collision system
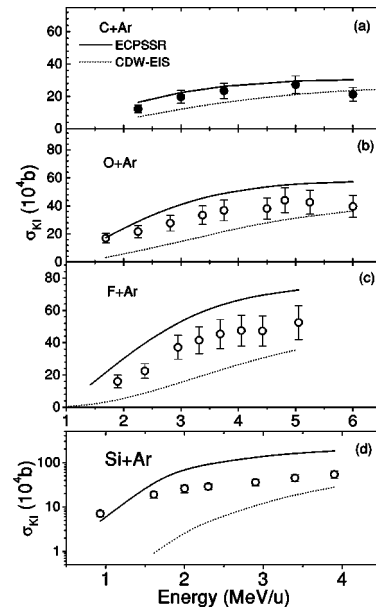


FIG. 6. The direct Coulomb ionization cross sections for Ar induced by C, O, F, and Si projectiles. The solid and the dotted lines represent the ECPSSR and CDW-EIS predictions, respectively. The data for Si+Ar are taken from Ref. [8].
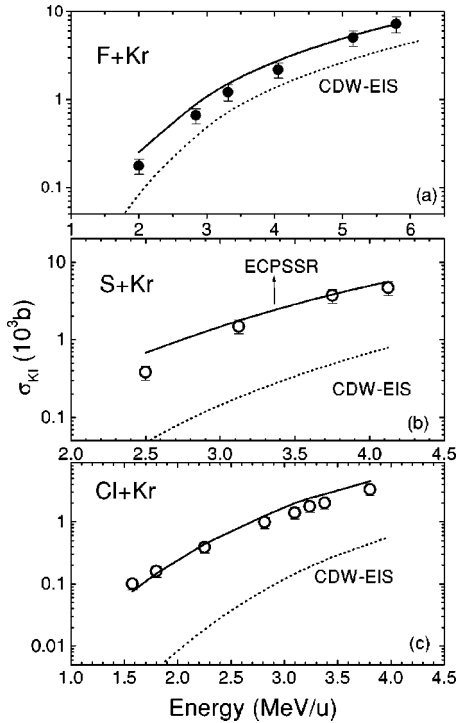
FIG. 7. Same as in Fig. 6, except for the Kr target bombarded by F, S, and Cl projectiles.



FIG. 8. The derived values of the single $K$-$K$ electron-transfer cross sections using H-like ions (filled symbols) for the Ar target using C, O, F, and Si [8] projectiles. The open symbols in (a) and (b) are derived by using bare ions. The solid and dotted lines represent the predictions of the close-coupling (CC) calculations, and the PSS model of Lapicki and McDaniel [21], respectively.

C+Ar ($S_z = 0.33$) the ECPSSR model gives a reasonable agreement with the data, overestimating only by about 10%. With increasing $S_z$ the ECPSSR calculations begin to overestimate the data by an increasing amount. For example, in the case of O+Ar and F+Ar ($S_z = 0.44$ and 0.55), the calculations overestimate the data by about 25–30%. In the case of nearly symmetric collision partners Si+Ar ($S_z = 0.78$) the calculations overestimate the cross sections by a factor as large as 3–4 at the higher energies. In Figs. 7(a)–7(c), we show the ionization cross-section data for F+Kr, S+Kr and Cl+Kr, i.e., $S_z$ varying in the range of 0.25 and 0.5. The F+Kr ($S_z = 0.25$) and S+Kr ($S_z = 0.44$) data show a better agreement with the calculations, especially in the higher-energy range, an observation quite similar to the case of C+Ar [Figs. 6(a) and 6(b)]. In collision systems with a slightly higher symmetry parameter ($S_z = 0.48$), i.e., Cl+Kr, the calculations agree with the data in the lower-energy part (i.e., 2.5 MeV/u), above which it starts to deviate, an observation consistent with that for F+Ar [Fig. 6(c)]. It is clear from this analysis, as well as from previous measurements with lighter ions like $p$ and He$^+$, that the ECPSSR model can barely explain the total cross section data for $S_z \lesssim 0.33$. For slightly more symmetric collisions the theory starts to deviate. It should be noted that the difference between the ECPSSR calculations and the data increases with the energy for higher values of $S_z$, which is contrary to the general expectation as far as perturbative methods are concerned.

The CDW-EIS calculations, on the other hand, underestimate our data in most cases, and come closer to the data only for the asymmetric collisions C+Ar [Fig. 6(a)], for which it underestimate the data by about 20–30%. The situation is somewhat similar for O, F+Ar giving a deviation of about
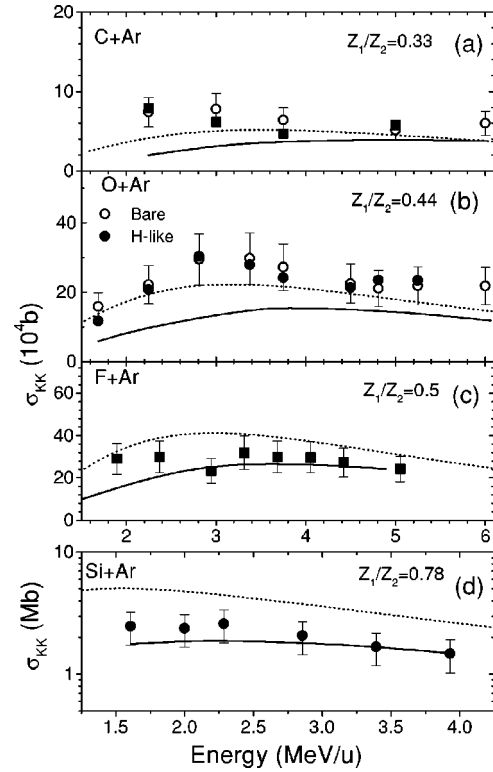
20–50%. A much larger deviation from the data is to be noted for Si+Ar. However, the theory asymptotically approaches the data in the high-energy limit, an observation consistent with the perturbative method. It is obvious that this model breaks down drastically for higher $Z$ targets such as for Kr (see Fig. 7), in which case the theory largely underestimates (by a factor of about 1.5) even for the most asymmetric system F+Kr [Fig. 7(a)]. Large deviations in more symmetric collisions with S and Cl are clearly observed [Figs. 7(b) and 7(c)]. It is also not clear from the present measurement whether the theory approaches the data in the high-energy limit or not.

As mentioned earlier, the CDW-EIS approach which takes care of the two-center effect, explains the double differential and total ionization cross-section data quite well for light targets like H and He in collision with fast bare heavy ions [16–19]. For these collision systems, involving only loosely bound outer-shell electrons, it is customary to define the perturbation strength parameter as $S_p = Z_p / v_p$ in order to characterize the post-collision interaction and the validity of different theoretical models [32]. The CDW-EIS approach was shown to explain the ionization dynamics quite well for $S_p$ values varying between 0.4 and 1, and the scaled velocity parameter $v_r \gg 1$. In the case of inner-shell processes, however, the binding energy needs to be included in the definition of such a strength parameter, as indicated by Tiwari *et al.* [33] for $K$-shell excitation. In the present cases the pro-

TABLE I. Derived values of the $K$ ionization ($\sigma_{KI}$) and the $K$-$K$ electron-transfer cross sections for different collision systems at various energies. The absolute errors in the cross sections are about 25–30 %.

| Collision | Energy | $\sigma_{KI}$ ($10^4$ b) | $\sigma_{KK}$ ($10^4$ b) | Collision | Energy | $\sigma_{KI}$ (b) | $\sigma_{KK}$ (b) |
|---|---|---|---|---|---|---|---|
| C + Ar | 27 | 12.3 | 7.9 | F+Kr | 38 | 176 | |
| | 36 | 22.4 | 6.2 | | 54 | 659 | 220 |
| | 45 | 23.4 | 4.7 | | 63 | 1214 | 343 |
| | 60 | 27.2 | 5.8 | | 77 | 2176 | 1153 |
| | 72 | 21.3 | 6.0 | | 98 | 5041 | 1127 |
| | | | | | 110 | 7210 | 1480 |
| O + Ar | 27 | 17.0 | 11.7 | S+Kr | 80 | 380 | |
| | 36 | 21.7 | 20.8 | | 100 | 1480 | 2770 |
| | 45 | 27.7 | 30.4 | | 120 | 3700 | 6610 |
| | 54 | 33.4 | 27.9 | | 132 | 4650 | 14100 |
| | 60 | 36.8 | 24.2 | | | | |
| | 72 | 38.1 | 21.3 | | | | |
| | 77 | 44.0 | 23.5 | | | | |
| | 84 | 42.6 | 23.4 | | | | |
| | 96 | 39.6 | 21.8 | | | | |
| F + Ar | 36 | 20 | 29.0 | Cl+Kr | 56 | 100 | |
| | 45 | 22.4 | 30.0 | | 64 | 160 | |
| | 56 | 37.1 | 23.4 | | 80 | 390 | 2140 |
| | 63 | 41.5 | 31.9 | | 100 | 980 | 2730 |
| | 70 | 45.3 | 29.9 | | 110 | 1400 | |
| | 77 | 47.5 | 29.7 | | 115 | 1770 | 5962 |
| | 84 | 47.2 | 27.3 | | 120 | 1996 | 5450 |
| | 96 | 52.4 | 24.2 | | 135 | 3285 | 9030 |

jectile velocity is quite small compared to the orbital velocity of the active electron, i.e., $v_r \leqslant 1$, varying between 0.2 and 1.0 for Ar. In the case of Kr target $v_r \leqslant 1$, varying between 0.25 and 0.4, indicating an adiabatic collision. In this region, different collision channels such as capture, ionization, and excitation become comparable (see Table I), and the perturbative models become less accurate [34]. More elaborate coupled-channel approaches are necessary which can treat the target and the projectile field on equal footing, and also can account for strong coupling among the reaction channels. The two-center effect on the ionized electron is expected to be much stronger in the present case as compared to the collisions with light targets since the electron feels a much stronger field arising from the (multiply) ionized heavy target atom in the post collision regime. CDW-CDW calculations were also carried out, but they show deviations similar to the CDW-EIS one.

The measured $K$-$K$ electron-transfer cross sections (per $K$ vacancy) are shown in Fig. 8 for the Ar target. They exhibit a broad maximum at around 2–2.5 MeV/u, and then decrease with energy. The similar data for the Kr target is shown in Fig. 9. The data derived from the H-like (solid circles) and the bare ions (open circles) agree very well, as shown in the case of the O+Ar collision system [Fig. 8(b)]. The two-center close-coupling calculations are presented to compare with the experiment for different symmetry parameters. It can be seen that for the asymmetric collision C+Ar the theory underestimates the data largely in the lower-energy

region, and tends to agree with the data (within 20–25%) only at higher energies. With increasingly symmetric collisions (e.g., O+Ar and F+Ar) the agreement with the data becomes better. For F+Ar the calculations reproduce the data quite well except below 2 MeV/u. In the case of nearly symmetric collisions Si+Ar, however, the close-coupling calculations provide an excellent agreement with the data. Therefore, as far as the Ar target is concerned, the agreement with the close-coupling theory is good for symmetric collision systems. In case of the Kr target the theoretical curve crosses over the data at around 3.5 or 4 MeV/u. For the asymmetric collision F+Kr, the theory overestimates the data at the lowest energy, and underestimates at higher energies by almost a factor of 2. For S+Kr the deviations still exist, though they are slightly reduced at lower energy. For the relatively symmetric collision Cl+Kr the deviations are further reduced, and the calculations reproduce almost all the data within the experimental errors (20–25 %). It may be concluded that close-coupling calculations reproduce the $K$-$K$ electron-transfer cross sections for near symmetric collisions, and provide an increasingly greater deviation from the data with more asymmetric collision systems. To improve the agreement in the case of asymmetric collisions more states were included in the calculations, but the situation did not seem to change. Since the projectile velocity in many cases was less than the target $K$-electron orbital velocity, molecular orbitals were also included in the calculations, which again did not help to improve the agreement.
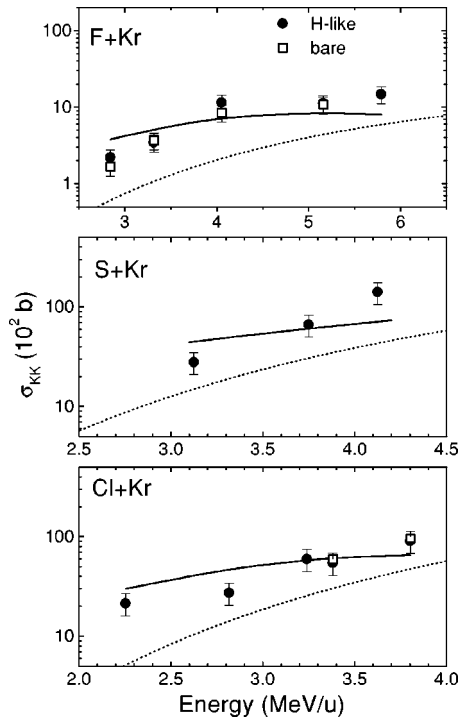
FIG. 9. Same as in Fig. 8, except for the Kr target bombarded by F, S, and Cl.



FIG. 10. The derived values of the *K-L* electron-transfer cross sections per *L* vacancy for Cl+Kr (a) and S+Kr (b) as a function of the projectile energy. The solid line is the calculation by Lapicki and McDaniel [21].

The perturbed stationary-state calculations of Lapicki and McDaniel [21] were carried out, and it was found that these calculations give a reasonable agreement with the data for most asymmetric collisions such as C+Ar and O+Ar, while they overestimate slightly for the F+Ar data (dotted lines in Fig. 8). The calculations show a greater deviation from the data with increasing symmetry parameter. For example, in the case of Si+Ar the calculation overestimates the experimental data by a factor of $\sim 2$. In the case of collisions with heavier targets like Kr, the calculations by Lapicki and McDaniel underestimate the experimental data (Fig. 9) by a larger factor (of about 2–4), and approach the data at higher energies. The energy dependences are reproduced quite well. However, this method, although not an *ab initio* one, works better for asymmetric collisions involving lighter targets, and can be used to estimate the inner-shell transfer cross sections for practical design of experiments.

The derived values of *K-L* electron-transfer cross sections (per *L* vacancy) are plotted in Fig. 10 for Cl+Kr. The measured cross sections are found to increase with the beam energy. The calculated values using the model of Lapicki and McDaniel are also shown in the same figure. Though the measured values are considerably higher than the calculated ones, nevertheless, the relative variation with energy is well reproduced by the calculation.

## IV. CONCLUSIONS

We have presented a combined and systematic study of *K* ionization and state-selective *K-K* electron-transfer cross sections for Ar and Kr targets by varying the symmetry parameter of the collisions in the energy range of 1.5–6.0
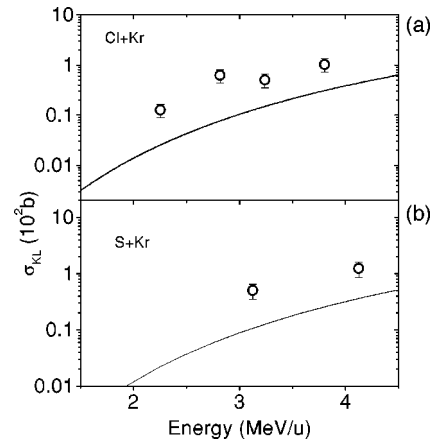
MeV/u. The *K*-*K* electron transfer and the *K* ionization cross sections derived for C-O-F–Si+Ar, F-S–Cl+Kr are used to provide a stringent test for first-order perturbative, continuum-distorted-wave, and close-coupling calculations. It was found that the CDW-EIS approach fails to reproduce *K* ionization cross sections at intermediate or lower energies, and largely underestimates the data for relatively symmetric collisions for which the two-center effect is supposed to be stronger. The deviation seems to be much larger for heavier target atoms like Kr as compared to Ar. The perturbed stationary-state calculations (ECPSSR) of Brandt and Lapicki overestimate the data except for most asymmetric collisions, for which a good agreement was found. In the case of the *K-K* electron-transfer process, the close-coupling calculations are found to deviate for the asymmetric collisions, and give a very good agreement for nearly symmetric collisions. The perturbed stationary-state calculations of Lapicki and McDaniel, on the other hand, explain the *K-K* electron-transfer data for asymmetric systems with lighter targets, and deviates for near-symmetric collisions. For heavier targets these calculations underestimate both the *K-K* and *K-L* electron-transfer cross sections. The shifts of the target *K* x-ray lines are studied as a function of the projectile charge states and energies to study the enhancement in the *K*-shell fluorescence yields as a result of multiple vacancies in the outer shells of the target atoms.

[1] A.S. Schlachter, J.W. Stearns, W.G. Graham, K.H. Berkner, R.V. Pyle, and J.A. Tanis, Phys. Rev. A **27**, 3372 (1983).

[2] H. Knudsen, H.K. Haugen, and P. Hvelplund, Phys. Rev. A **23**, 597 (1981).

[3] J. Hall *et al.*, Phys. Rev. A **33**, 914 (1986); **28**, 99 (1983).

[4] K. Wohrer, A. Chetioui, J.P. Rozet, A. Jolly, and C. Stephan, J. Phys. B **17**, 1575 (1984).

[5] L.C. Tribedi, K.G. Prasad, P.N. Tandon, Z. Chen, and C.D. Lin, Phys. Rev. A **49**, 1015 (1994); L.C. Tribedi, K.G. Prasad, and P.N. Tandon, *ibid.* **47**, 3739 (1993).

[6] J.A. Tanis, S.M. Shafroth, J.E. Willis, and J.R. Morwat, Phys. Rev. Lett. **45**, 1547 (1980).

[7] T J. Gray, in *Methods of Experimental Physics*, edited by P. Richard (Academic, New York, 1980), Vol. 17, p. 193.

[8] B.B. Dhal, *et al.*, J. Phys. B **33**, 1069 (2000).

[9] W. Brandt and G. Lapicki, Phys. Rev. A **23**, 1717 (1981), and references therein.

[10] G. Basbas, W. Brandt, and R. Laubert, Phys. Rev. A **17**, 1655 (1978).

[11] I.M. Chesire, Proc. Phys. Soc. London **84**, 89 (1964).

[12] Dź. Belkic, J. Phys. B **11**, 3529 (1978).

[13] D.S.F. Crothers and J.F. McCann, J. Phys. B **16**, 3229 (1983).

[14] P.D. Fainstein, V.H. Ponce, and R.D. Rivarola, J. Phys. B **24**, 3091 (1991).

[15] L. Gulyás, P.D. Fainstein, and A. Salin, J. Phys. B **28**, 245 (1995).

[16] J.O.P. Pedersen, P. Hvelplund, A. Petersen, and P. Fainstein, J. Phys. B **24**, 4001 (1991).

[17] N. Stolterfoht, H. Platten, G. Schiwietz, D. Schneider, L. Gulyás, P.D. Fainstein, and A. Salin, Phys. Rev. A **52**, 3796 (1995).

[18] L.C. Tribedi, P. Richard, Y.D. Wang, C.D. Lin, L. Gulyás, and M.E. Rudd, Phys. Rev. A **58**, 3619 (1998).

[19] L.C. Tribedi, P. Richard, W. DeHaven, L. Gulyás, M.W. Gealy, and M.E. Rudd, J. Phys. B **31**, L369 (1998).

[20] V.S. Nikolaev, Zh. Éksp. Teor. Fiz. **51**, 1263 (1966) [Sov. Phys. JETP **24**, 847 (1967)].

[21] G. Lapicki and F.D. McDaniel, Phys. Rev. A **22**, 1896 (1980).

[22] Jiyun Kuang and C.D. Lin, J. Phys. B **29**, 1207 (1996).

[23] W. Fritsch and C.D. Lin, Phys. Rep. **202**, 1 (1996).

[24] D.R. Bates and R. McCarroll, Proc. R. Soc. London, Ser. A **245**, 175 (1958).

[25] F. Hopkins, R. Brenn, R. Whittemore, N. Cue, V. Dutkiewicz, and R.P. Chaturvedi, Phys. Rev. A **13**, 74 (1976).

[26] J.A. Bearden, Rev. Mod. Phys. **39**, 78 (1967).

[27] C.P. Bhalla, Phys. Rev. A **8**, 2877 (1973).

[28] Y.K. Kim and M. Inokuti, Phys. Rev. A **3**, 665 (1971).

[29] H. Knudsen, L.H. Andersen, P. Hvelplund, G. Astner, H. Cederquist, H. Danared, L. Liljelsy, and K.-G. Rensfelt, J. Phys. B **17**, 3545 (1984).

[30] H. Berg *et al.*, J. Phys. B **25**, 3655 (1992).

[31] B. Bapat and E. Krishnakumar, Phys. Rev. A **55**, 3937 (1997).

[32] R.E. Olson *et al.*, Phys. Rev. A **58**, 270 (1998).

[33] U. Tiwari, A.K. Saha, L.C. Tribedi, M.B. Kurup, P.N. Tandon, and L. Gulyás, Phys. Rev. A **58**, 4494 (1998).

[34] R.K. Janev, L.P. Presnyakov, and V.P. Shevelko in *Physics of Highly Charged Ions*, Springer Series on Electrophysics Vol. 13 (Springer-Verlag, Berlin, 1985).